ACSNANO

www.acsnano.org

ARTICLE

Tailoring the Electrical Characteristics of MoS_2 FETs through Controllable Surface Charge Transfer Doping Using Selective Inkjet Printing

Inho Jeong, Kyungjune Cho, Seobin Yun, Jiwon Shin, Jaeyoung Kim, Gyu Tae Kim,* Takhee Lee,* and Seungjun Chung*

Cite This: *ACS Nano* 2022, 16, 6215–6223

Read Online

ACCESS | Metrics & More | Article Recommendations | Supporting Information

ABSTRACT: Surface charge transfer doping (SCTD) has been regarded as an effective approach to tailor the electrical characteristics of atomically thin transition metal dichalcogenides (TMDs) in a nondestructive manner due to their two-dimensional nature. However, the difficulty of achieving rationally controlled SCTD on TMDs *via* conventional doping methods, such as solution immersion and dopant vaporization, has impeded the realization of practical optoelectronic and electronic devices. Here, we demonstrate controllable SCTD of molybdenum disulfide (MoS_2) field-effect transistors using inkjet-printed benzyl viologen (BV) as an n-type dopant. By adjusting the BV concentration and the areal coverage of inkjet-printed BV dopants, controllable SCTD results in BV-doped MoS_2 FETs with elaborately tailored electrical performance. Specifically, the suggested solvent system creates well-defined droplets of BV ink having a volume of ~2 pL, which allows the high spatial selectivity of SCTD onto the MoS_2 channels by depositing the BV dopant on demand. Our inkjet-printed SCTD method provides a feasible solution for achieving controllable doping to modulate the electrical and optical performances of TMD-based devices.

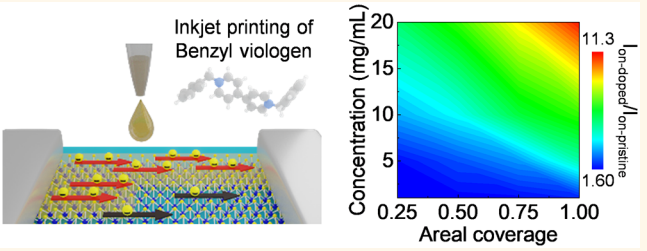

KEYWORDS: *molybdenum disulfide, chemical doping, surface charge transfer doping, inkjet printing, field-effect transistor*

Atomically thin two-dimensional (2D) transition metal dichalcogenides (TMDs) have emerged as building blocks for implementing next-generation nanoelectronics.[1−3] Among TMDs, layered molybdenum disulfide (MoS_2) has gained great attention due to its high carrier mobility, chemical and thermal stability, absence of dangling bonds, and tunable electronic energy band depending on the number of layers.[4−6] Specifically, chemical vapor deposition (CVD)-grown monolayer MoS_2 offers promising opportunities to realize large-area functional applications such as field-effect transistors (FETs) and optoelectronic devices.[7−10] For practical applications beyond laboratory-scale devices, the capability to tune the electrical characteristics of MoS_2 is important in building integrated logic circuits.[11−13] For mature three-dimensional (3D) Si-based semiconductor devices, thermal diffusion and ion implantation doping have been widely employed to facilitate the rational modulation of electrical characteristics.[13,14] However, these approaches have limitations when introduced to 2D TMDs because they can result in undesirable lattice distortion, a substantial number of defects, and doping instability.[14,15] Therefore, it is necessary to develop appropriate doping strategies for TMDs to modulate their electrical characteristics without deteriorating their intrinsic properties.

Recently, surface charge transfer doping (SCTD), which can induce electron donation or withdrawal between the deposited dopants and host TMDs, has been intensively investigated.[16−29] The carrier concentration of TMDs can be controlled by the SCTD without the lattice distortion of host TMDs. Various organic dopants have been reported to conduct SCTD on TMDs, such as tetrafluoro-

Received: January 2, 2022
Accepted: March 30, 2022
Published: April 4, 2022

https://doi.org/10.1021/acsnano.2c00021
ACS Nano 2022, 16, 6215–6223

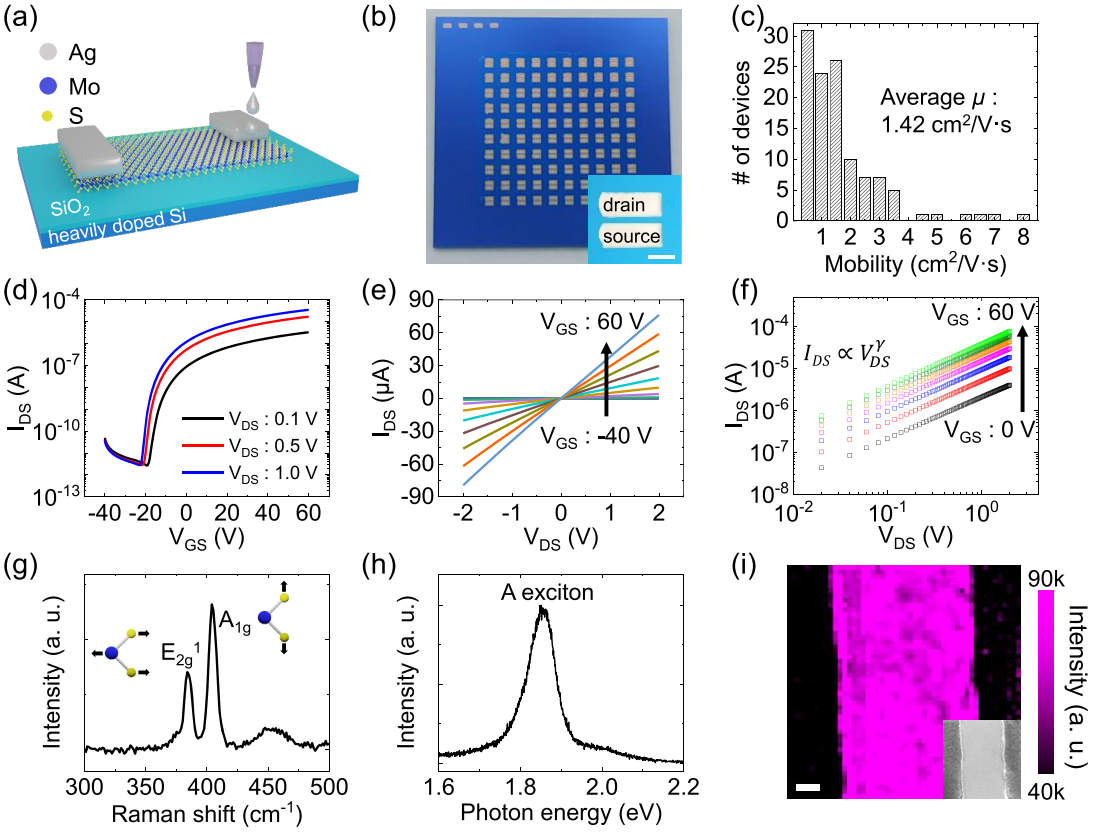

Figure 1. (a) Schematic of the MoS_2 FETs with inkjet-printed Ag contacts. (b) Optical images of the 10 × 10 MoS_2 FET array. Inset image shows a single MoS_2 FET. The scale bar is 200 μm. (c) Histogram of the field-effect mobility distribution of the MoS_2 FETs. (d) I_{DS}–V_{GS} curves and (e) I_{DS}–V_{DS} of the transferred monolayer MoS_2 FETs. (f) Logarithmic scale plot for I_{DS}–V_{DS} of MoS_2 FETs with an average γ value. (g) Raman spectra showing the E_{2g}^1 and A_{1g} modes, (h) PL spectra containing the A exciton peak, and (i) PL mapping image containing the A exciton peak at 1.84 eV. The inset indicates the optical image of the measured MoS_2 FET. The scale bar is 10 μm.

tetracyanoquinodimethane (F_4-TCNQ),[16,17] CF_3-terminated thiol,[18] $AuCl_3$,[19] and octadecyltrichlorosilane[20,21] for p-type dopants and nicotinamide adenine dinucleotide,[16] MgO,[22] aminopropyltriethoxysilane,[21] NH_2-terminated thiol,[18] LiF,[23] hydrazine,[24] *p*-toluenesulfonic acid,[25] chloride molecules,[26] potassium,[27] and benzyl viologen (BV)[28] for n-type dopants. Among these candidates, BV has been widely proposed as a promising chemical doping material for n-type TMDs because it acts as an electron donor due to the difference in energy level between the reduction potential and the vicinity of the conduction band edge of TMDs.[28,29] Moreover, its excellent environmental stability provides a high degree of freedom from the perspective of manufacturing. For performing SCTD, organic dopants are typically deposited onto the surface of TMDs *via* simple solution immersion or dopant vaporization for a long time.[20,21,24,27,28] However, it is difficult to conduct chemical doping with high spatial selectivity on demand in these approaches, which is of fundamental importance to implement integrated circuit applications. Many studies based on conventional lithography have been carried out to enable selective chemical doping of TMDs. Laterally created 2D heterojunctions have been demonstrated by employing selective plasma treatments onto a MoS_2 flake with a spatially covered photoresist (PR) layer.[30] Additionally, selective chemical doping has been delivered with partially covered hexagonal boron nitride (*h*-BN)[31] or *via* co-evaporation systems with a partially covered mask on TMDs.[29] Despite these efforts, new methodologies for introducing larger-area, spatially selective SCTD on TMDs without the need for undesirable masks, complex patterning, or vacuum processing are highly required.

Additive manufacturing, especially in inkjet printing, can be a potential candidate due to its high-resolution, maskless, and drop-on-demand patterning ability with ink droplets having a volume of a few pL; therefore, precisely controlled selective doping can be performed on TMDs. There have been results of chemical doping *via* inkjet printing on oxide, organic, and carbon nanotube (CNT) thin-film transistors (TFTs) and their logic applications.[32−34] However, to the best of our knowledge, none have been reported for SCTD with inkjet-printed organic dopants on TMDs, even though efficient chemical doping is expected due to their high surface-to-volume ratio and atomically thin nature.

Herein, we demonstrate exquisitely controlled SCTD with BV inks for enhancing the electrical performance of CVD-grown MoS_2 FETs using spatially selective inkjet printing. The fluid characteristics of the BV ink are carefully optimized, which allows the creation of pL-scale ink droplets without satellites and results in a well-defined doping area on the MoS_2 channels. By exploiting the attractive merits of BV, inkjet-printed SCTD provides competitive doping effects to MoS_2 FETs, exhibiting efficient modulation of their electrical characteristics when compared with conventional chemical doping methods based on solution immersion and vaporization. Most importantly, drop-on-demand inkjet printing can directly deliver spatially controlled SCTD effects by selectively

https://doi.org/10.1021/acsnano.2c00021
ACS Nano 2022, 16, 6215−6223

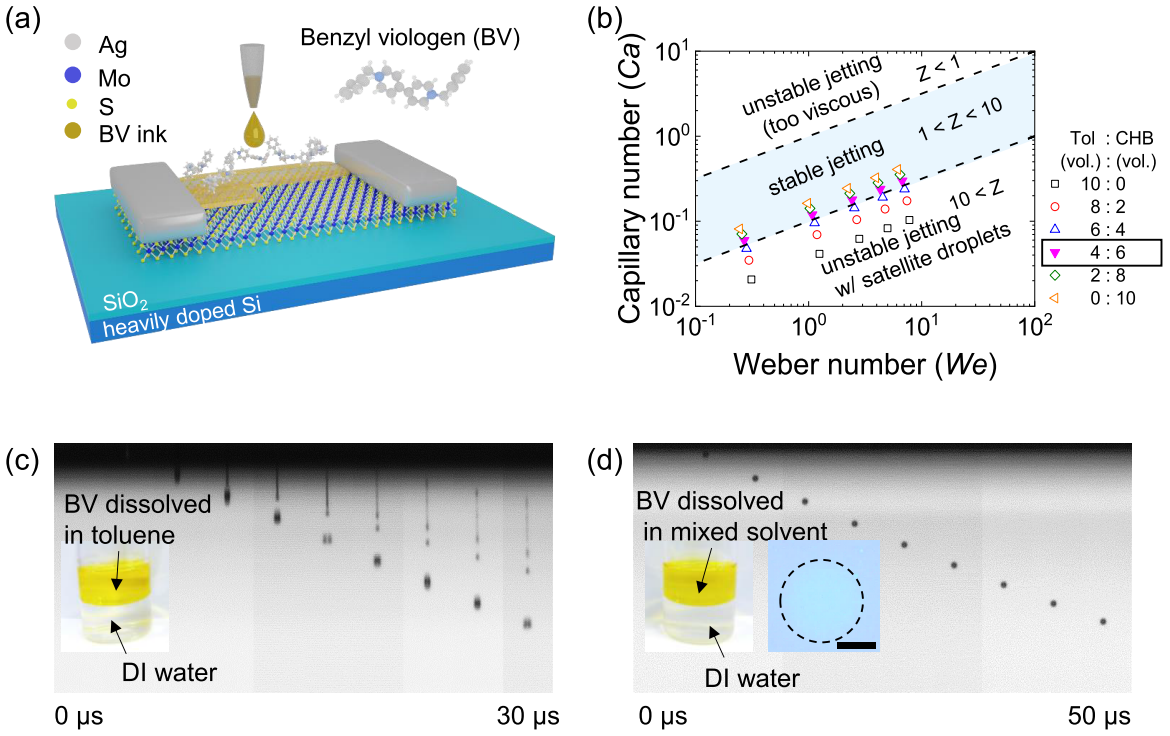

Figure 2. (a) Schematic of the SCTD process on a MoS_2 FET using inkjet printing. (b) Stable inkjettability window of the BV inks based on the capillary number (*Ca*)−Weber number (*We*) relationship of the toluene and cyclohexylbenzene mixtures. Time evolution of an ink droplet in flight after ejection from a nozzle for (c) BV ink based on toluene and (d) BV inks based on the toluene and cyclohexylbenzene mixture at a 4:6 ratio. The concentration of both BV inks is 5 mg/mL. An image of a single BV ink droplet on the MoS_2 film by inkjet printing is also included in the inset. The scale bar is 20 μm.

depositing BV dopants on MoS_2 channels at different dopant concentrations. The changes in the electrical characteristics of MoS_2 FETs, the shifts in Raman spectroscopy peak positions, the decrease in photoluminescence (PL) intensity, and the blue shift of the XPS binding energy of BV-doped MoS_2 all support that controlling inkjet-printed SCTD depends on the BV concentration and the areal coverage of BV dopants. Our results demonstrate high potential for constructing 2D homojunctions in TMD films or complementary logic devices through the integration of SCTD-assisted 2D TMD-based FETs.

RESULTS AND DISCUSSION

Figure 1a and b show the schematic of a MoS_2 FET with inkjet-printed Ag source/drain (S/D) electrodes and the optical image of the FET arrays. CVD-grown monolayer MoS_2 films were transferred onto 300-nm-thick SiO_2/heavily doped Si substrates using the poly(methyl methacrylate) (PMMA)-mediated transfer method.[35] For the formation of S/D contacts, a nanoparticle-type Ag ink was directly printed onto the MoS_2 channels without any surface treatment. Note that inkjet printing does not require procedures that are unfavorable to TMDs, such as residual chemical deposition and ultraviolet (UV) exposure.[36] Further details are described in the Methods section. The histogram of the field-effect mobility of the fabricated CVD-grown MoS_2 FETs with the inkjet-printed Ag electrode is shown in Figure 1c; notably, they are comparable to the field-effect mobility of conventional CVD-grown MoS_2 FETs fabricated by standard lithography.[37] Figure 1d and e show the representative transfer (source−drain current *versus* gate voltage, I_{DS}−V_{GS}) and output (drain−source current *versus* drain voltage, I_{DS}−V_{DS}) characteristics of the CVD-grown MoS_2 FETs with inkjet-printed Ag contacts. All electrical characterization was conducted in a vacuum at room temperature. From the transfer curve in Figure 1d, the field-effect mobility (μ) and 2D carrier density (n_{2D}) can be calculated and are defined as[28,38]

$$\mu = \left(\frac{\partial I_{DS}}{\partial V_{GS}}\right)\frac{L}{W}\frac{1}{C_{OX}V_{DS}} \quad (1)$$

$$n_{2D} = I_{DS}\frac{L}{W}\frac{1}{q\mu V_{DS}} \quad (2)$$

where $\partial I_{DS}/\partial I_{GS}$, W, L, C_{OX}, and q denote the transconductance, channel width, channel length, gate oxide capacitance, and electron charge, respectively. The extracted μ, on/off ratio, subthreshold swing (SS), threshold voltage (V_{th}), and n_{2D} are ~7.64 $cm^2/V{\cdot}s$ at V_{DS} = 60 V, 10^7, 1.38 V/decade, −13.1 V, and 2.6 × 10^{12} cm^{-2}, respectively. Specifically, in the logarithmic scale plot for I_{DS}−V_{DS} measured at V_{GS} ranging from 0 to 2 V, the extracted average linearity parameter $\gamma \sim 1$ indicates nearly ohmic contacts between the transferred MoS_2 channel and printed Ag contacts (Figure 1f). The quality of the transferred MoS_2 films was also evaluated by Raman and PL spectroscopy analysis (Figure 1g and h). The difference in wavenumber (~20 cm^{-1}) between the in-plane E_{2g}^1 and out-of-plane A_{1g} Raman peaks, the distinct PL peak at ~670 nm (corresponding to ~1.84 eV), and the PL mapping results of the channel region support that the transferred MoS_2 film is a uniformly grown monolayer (Figure 1i).[39−43]

Typically, BV molecules were dissolved into deionized water and became BV^{2+}; then, nonpolar solvents and sodium borohydride were sequentially added into the BV solution as

https://doi.org/10.1021/acsnano.2c00021
ACS Nano 2022, 16, 6215−6223

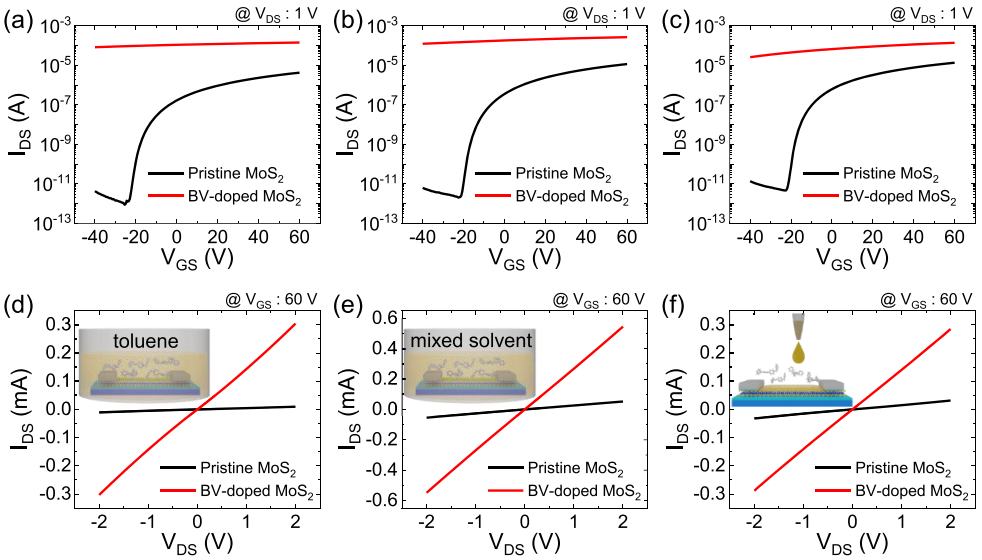

Figure 3. I_{DS}−V_{GS} and I_{DS}−V_{DS} of MoS_2 FETs with and without SCTD conducted by (a, d) immersion in BV inks based on toluene for 3 h, (b, e) immersion in BV inks based on the toluene and cyclohexylbenzene mixture at a 4:6 ratio for 3 h, and (c, f) inkjet printing with BV inks based on the toluene and cyclohexylbenzene mixture at a 4:6 ratio. The concentrations of the BV inks are 5 and 20 mg/mL for immersion and inkjet printing, respectively.

a catalyst. After the redox reactions, BV^{2+} is reduced to hydrophobic BV^0, allowing its separate transfer from water to nonpolar solvents. More details are described in the Methods section. The conduction band edge (E_C) of MoS_2 is located at ~0 V *versus* the standard hydrogen electrode,[44,45] while the reduction potentials of the BV molecule throughout the two successive redox reactions from BV^+ to BV^0 and from BV^{2+} to BV^+ are equal to −0.79 and −0.33 V, respectively (Figure S1 in the Supporting Information).[46] Due to the band offset where the reduction potential of the BV molecule is positioned below the E_C edge of MoS_2, electrons can be transferred from the neutral BV^0 to the MoS_2 channel, resulting in a significant increase in carrier concentration.

To selectively conduct SCTD with BV onto CVD-grown MoS_2 channels *via* inkjet printing as shown in Figure 2a, rheologically apposite BV inks need to be prepared to achieve high-quality inkjet printing that is closely related to the resolution of the doping area. One of the most critical factors is to create stable ink droplets having volumes of a few pL with excellent inkjetability, which can be estimated by the Ohnesorge number (Oh). Oh can be calculated from three dimensionless parameters, namely, the Reynolds number (Re), Weber number (We), and capillary number (Ca), which are determined by the fluidic properties of inks, including their viscosity, surface tension, density, and inertial force.

$$Re = \frac{\text{inertial force}}{\text{viscous force}} = \frac{\rho v d}{\eta} \tag{3}$$

$$We = \frac{\text{inertial force}}{\text{surface tension force}} = \frac{\rho v^2 d}{\gamma} \tag{4}$$

$$Ca = \frac{\text{viscous force}}{\text{surface tension force}} = \frac{\eta v}{\gamma} \tag{5}$$

$$Oh = \frac{\text{viscous force}}{\sqrt{\text{inertial force} \times \text{surface tension}}} = \frac{\eta}{\sqrt{\sigma \rho d}} \tag{6}$$

where ρ is the density of the ink, v is the velocity of the ink, d is the nozzle diameter, η is the viscosity of the ink, and γ is the surface tension of the ink. It is well known that the inverse of Oh (Z) ranging from 1 to 10 can be a criterion for reliable inkjettability without undesirable satellite droplets.[47−49] Although toluene has been widely used to prepare a BV ink as a nonpolar solvent, it is unfavorable to form well-defined inkjet droplets with a Z value of ~27, resulting in unstable inkjetting, as shown in Figure 2c. To address this issue, we modified the solvent system of BV ink while simultaneously considering BV solubility and inkjettability. Cyclohexylbenzene (CHB) can be a promising candidate as an additive due to its high compatibility with toluene, apposite Z value of 6.45, and high boiling point of 238 °C, all of which lead to reliable inkjetting.[50,51] Furthermore, the CHB−toluene mixed solvent (simply denoted as the mixed solvent) promotes more uniformly deposited BV layers by competing for the Marangoni effect and capillary action (Figure S3 in the Supporting Information). Therefore, BV ink was dissolved in the mixed solvent to meet the requirements mentioned above (Figure 2b). From the theoretical design and experimental results, a 4:6 volume ratio of toluene to CHB is determined with a Z value of 8.98, as shown in Table S1 in the Supporting Information. Our solvent system produces well-defined and stable BV ink droplets with a volume of ~2 pL (Figure 2d), and these droplets form a circular pattern with a diameter of ~40 μm on the MoS_2 channel.

To investigate the compatibility of the CHB−toluene mixture as a solvent of BV ink and inkjet printing to deliver the n-type doping effects, SCTD was conducted on CVD-grown MoS_2 FETs *via* three methods: immersion in a BV ink based on toluene, immersion in a BV ink based on the mixed solvent, and inkjet printing of BV ink based on the mixed solvent. These methods were followed by electrical characterization in a vacuum. Figure 3 shows the electrical characteristics of the MoS_2 FETs before and after SCTD, including the transfer curves (Figure 3a−c) and output characteristics (Figure 3d−f) for three methods. All three SCTD processes deliver consistent n-type doping effects to the MoS_2 FETs,

https://doi.org/10.1021/acsnano.2c00021
ACS Nano 2022, 16, 6215−6223

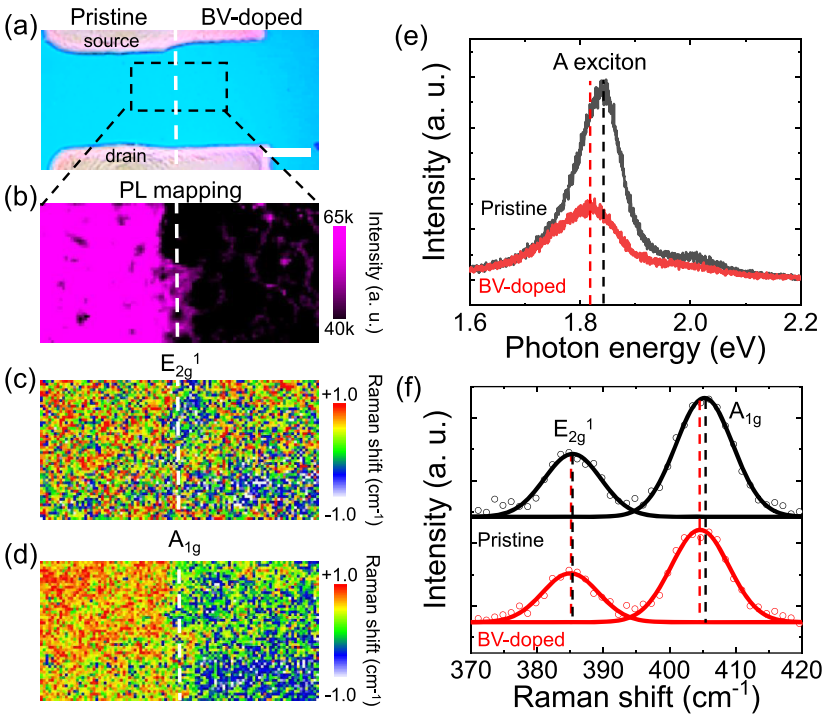

Figure 4. (a) Optical image of spatially selective BV-doped MoS_2 obtained by inkjet printing. (b) PL mapping image showing the peak intensity at a photon energy of 1.84 eV (A exciton). Raman mapping image of the Raman shift of the (c) E_{2g}^1 and (d) A_{1g} modes. (e) PL spectra of the pristine and BV-doped MoS_2 films. (f) Raman spectra of the pristine and BV-doped MoS_2 films. The symbols are experimental data, and the solid lines are the fitting results with a Gaussian function. The scan size of PL and Raman mapping is 100 μm × 200 μm. The concentration of BV inks is 5 mg/mL for SCTD on MoS_2. The scale bar is 100 μm.

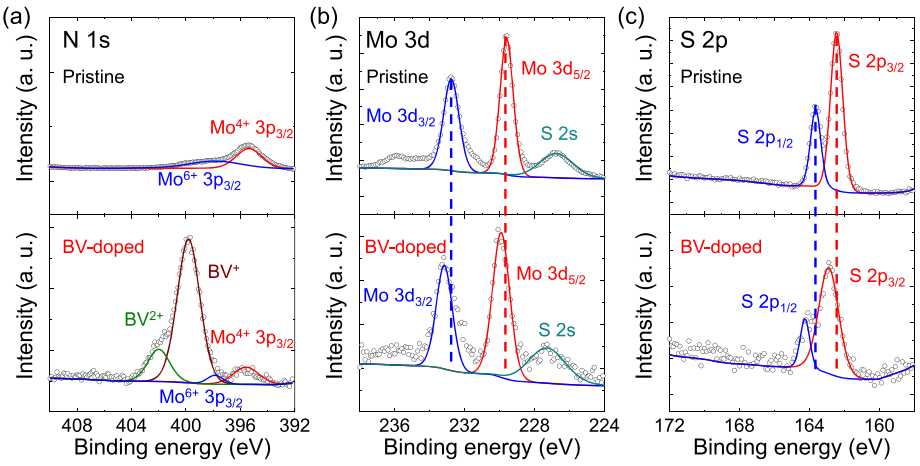

Figure 5. Deconvoluted XPS spectra of the pristine and BV-doped MoS_2 films for the (a) N 1s peaks, (b) Mo 3d and S 2s peaks, and (c) S 2p peaks. The symbols and solid lines are the experimental XPS data and deconvolution of the XPS spectra using the Gaussian function, respectively.

exhibiting a V_{th} shift toward the negative gate voltage direction and a significant increase in the field-effect mobility, on-state current, and carrier sheet density (Table S2 in the Supporting Information for details). These results support that the prepared BV inks for stable inkjet printing can be successfully introduced to modulate the electrical performance of MoS_2 FETs *via* spatially selective SCTD. The increase of electron mobility after doping could be attributed to the reduction of contact resistance and the screening effect of excess doped electrons.[19,23,26,28] Further improvements would be expected if remote modulation doping can be introduced onto 2D materials by suppressing charge impurity scattering in the channel.[52] It should also be noted that no significant change is observed in the electrical characteristics of MoS_2 FETs after immersion in the solvent only (without BV molecules) (Figure S4 in the Supporting Information).

The changes in the optoelectronic properties of MoS_2 after inkjet printing BV molecules were also investigated using Raman and PL spectroscopy. The BV ink was inkjet-printed with high spatial selectivity on the MoS_2 channel, as illustrated in Figure 4a. Figure 4b–d show the PL mapping and Raman mapping images of a specific region of MoS_2 film with and without inkjet-printed BV molecules indicated as a dashed box in Figure 4a. As shown in Figure 4b and e, the A exciton peak

https://doi.org/10.1021/acsnano.2c00021
ACS Nano 2022, 16, 6215–6223

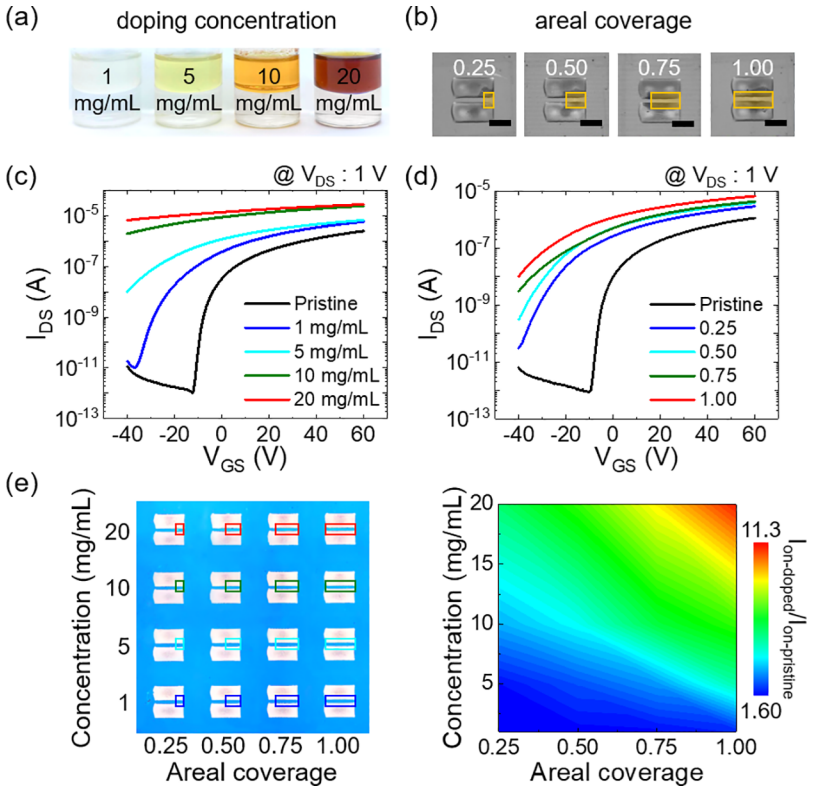

Figure 6. (a) Optical images of the BV inks with different BV concentrations. (b) Spatially selected SCTD with different areal coverages *via* inkjet printing. (c) Transfer curve of the BV-doped MoS_2 FET with different BV concentrations *via* inkjet printing. The areal coverage ratio is 1.00. (d) Transfer curve of the BV-doped MoS_2 FET with different areal coverages *via* inkjet printing. The concentration of BV ink is 5 mg/mL. (e) Optical image of the BV-doped MoS_2 FET array with different BV concentrations and areal coverage *via* spatially selective inkjet printing. The contour plot indicates the ratio of the on-state current of 80 BV-doped MoS_2 FETs as a function of the doping concentration and areal coverage at a fixed V_{DS} of 1 V and V_{GS} of 60 V. The scale bar is 200 μm.

of ~1.84 eV corresponding to the optical bandgap of monolayer MoS_2 is observed throughout the undoped area of MoS_2, while the BV-doped MoS_2 uniformly exhibits a decreased PL intensity with a red shift in the A exciton energy. This decrease in the A exciton arises from the suppression of radiative recombination by excess electrons due to chemical doping, consistent with the results in previous studies.[16,53,54] Likewise, the results of Raman spectroscopy also support the effect of inkjet-printed SCTD with BV. It is known that the out-of-plane A_{1g} is more sensitive to the presence of deposited molecular dopants on the surface of MoS_2 than the in-plane E_{2g}^1 due to stronger electron−phonon coupling.[42,43] We also observe that the A_{1g} peak shifts to the lower wavenumber direction, while the position of the E_{2g}^1 peak is unchanged after performing inkjet-printed SCTD, as shown in Figure 4f.

Furthermore, X-ray photoelectron spectroscopy (XPS) analysis reveals that the inkjet-printed BV dopant donates electrons to the underlying MoS_2 film. Figure 5a−c show the XPS spectra of the undoped MoS_2 (top) and BV-doped MoS_2 (bottom) films for Mo, S, and N, respectively. The XPS spectra show two distinctive photoelectron signals at binding energies of 399.8 and 402.0 eV related to N 1s after introducing the inkjet-printed BV; notably, these peaks are not observed on undoped MoS_2. Thus, these two peaks are attributed to viologen nitrogen radicals (BV^+) and positively charged viologen nitrogen radicals (BV^{2+}), which support electron donation from the inkjet-printed BV dopants.[55] In addition, the representative XPS peaks of MoS_2 shift toward a higher binding energy with inkjet-printed SCTD (Figure 5b and c), which indicates that the Fermi level of the MoS_2 energy band moves to the conduction band edge due to the transferred charges from the BV dopants to MoS_2.[56]

With the advantages of the BV inks and inkjet printing, we demonstrate elaborate control of the SCTD effect on the electrical performance of MoS_2 FETs by adjusting the dopant concentration and areal coverage of BV dopants. Figure 6a shows the BV inks dissolved in the mixed solvent with different dopant concentrations: 1, 5, 10, and 20 mg/mL. Because the CVD-grown MoS_2 channels have a high surface-to-volume ratio with a 2D nature, the SCTD effects are highly responsive to the areal coverage of BV dopants as well as the BV concentration. In this regard, the electrical characteristics of BV-doped MoS_2 FETs can be modulated by changing the deposited BV dopants with an areal coverage ratio of 0.25 to 1.00. This is feasible due to the high spatial resolution of well-optimized inkjet printing, which can achieve a scale of tens of μm on demand, as shown in Figure 6b. Figure 6c shows the transfer characteristics of pristine MoS_2 FETs and BV-doped MoS_2 FETs with different BV concentrations of 1, 5, 10, and 20 mg/mL by inkjet printing. As the dopant concentration increases, stronger n-type doping effects, such as a shift in V_{th} toward the negative gate voltage direction, are observed, which indicates a higher carrier concentration and an increase in the on-state current. Figure 6d shows the representative transfer curves of pristine MoS_2 FETs and BV-doped MoS_2 FETs with different areal coverages of BV dopants with a fixed BV concentration of 5 mg/mL. The controlled n-type doping effects depending on the BV concentration and the areal

https://doi.org/10.1021/acsnano.2c00021
ACS Nano 2022, 16, 6215−6223

coverages of BV dopants are summarized in Table S3 and Figure S5 in the Supporting Information. In previous studies, although many efforts have been dedicated to optimizing a doping process with different immersion times and concentrations of BV dopants, there are inherent limitations: it is difficult to deliver exquisitely controlled doping effects to MoS_2 FET arrays with high spatial selectivity on a single substrate. In this work, by adjusting the amount of dopants physically adsorbed to the MoS_2 channel *via* inkjet printing, we demonstrate an array of CVD-grown MoS_2 FETs selectively doped with different SCTD conditions on a single substrate. The contour plot indicates the gradually tailored on-state current of BV-doped MoS_2 FETs as a function of the doping concentration and areal coverage (Figure 6e).

CONCLUSIONS

In conclusion, we introduced controllable SCTD for tailoring the electrical characteristics of MoS_2 FETs using spatially selective inkjet printing. The solvent system to prepare inkjet-printable BV inks was optimized considering their fluid properties, which allowed high spatial selectivity and excellent inkjettability with well-defined droplets having a volume of a few pL. Inkjet-printed SCTD with BV delivered efficient n-type doping effects to MoS_2 FETs, achieving results that were comparable to those of SCTD conducted by using conventional solution immersion for a long time. Drop-on-demand inkjet printing and the high degree of freedom of BV concentrations enabled us to elaborately control SCTD to produce MoS_2 FETs with well-tailored electrical characteristics, which cannot be achieved *via* conventional chemical doping based on solution immersion and vaporization. The Raman and PL spectroscopy results could be evidence to support the SCTD effect of inkjet-printed BV dopants. We believe the suggested inkjet-printed SCTD method can be applied to other organic dopants if their solubility and stability in inkjet-printable solvents are guaranteed. Our study proposes a feasible solution for controllable SCTD using inkjet printing toward the realization of further practical TMD-based devices with efficiently tailored electrical characteristics.

METHODS

Procedure of MoS_2 FET Fabrication. Poly(methyl methacrylate) was spin-coated as a sacrificial layer onto a continuous CVD-grown monolayer MoS_2 film on a SiO_2/heavily doped silicon substrate (purchased from Six-Carbon Corp.), followed by hard baking on a 180 °C hot plate for 90 s. Then, thermal releasing supporting tape (purchased from Graphene Square) was directly attached to the PMMA-coated CVD-grown MoS_2 film. It was immersed in potassium hydroxide solution (KOH) at 60 °C to remove the SiO_2 layer, rinsed with deionized water, and dried with a N_2 gun. The PMMA-coated MoS_2 film was then transferred onto the target substrate and dried in a vacuum oven for 12 h. After removing the supporting tape through thermal treatment on a 120 °C hot plate, finally, the PMMA sacrificial layer was immersed in 60 °C acetone for 10 min to reproduce monolayer MoS_2 films. The electrical contacts were inkjet-printed directly on the transferred MoS_2 with nanoparticle-type Ag ink (DGP 40LT-15C, ANP Co. Ltd.). The silver ink was printed with a drop velocity of ∼3 m/s, drop frequency of 3 kHz, and drop spacing of 25 μm (1016 dpi) under a printing bed at 60 °C. After the source and drain electrodes were printed, they were annealed at 150 °C for 30 min on a hot plate. The electrical characteristics of the pristine MoS_2 FETs and doped MoS_2 FETs were measured using a semiconductor parameter analyzer (Agilent B1500A) under vacuum conditions.

Preparation of Benzyl Viologen Inks. Benzyl viologen dichloride powders were dissolved in 5 mL of deionized water followed by the addition of 5 mL of nonpolar solvent (pure toluene, the mixed solvent: toluene and cyclohexylbenzene at a 4:6 ratio) for a biphasic solution. Sodium borohydride powder (Sigma–Aldrich), which acted as a catalyst, was added to the nonpolar solvent–water biphasic solution. After storing for 1 day, the top nonpolar solution containing the BV dopant was extracted using a syringe. The chemical doping of MoS_2 FETs was conducted either by immersion into the BV solution for 3 h or inkjet printing of the BV ink. Then, BV-doped MoS_2 FETs were annealed at 120 °C for 1 h in a vacuum oven to eliminate residual solvents. All materials were purchased from Sigma–Aldrich Corp.

Characterization of the Pristine or BV-Doped MoS_2. Raman and PL spectroscopy were performed to investigate the optoelectronic properties of the MoS_2 film. Raman spectroscopy was performed using an XperRam 200 instrument (Nanobase, Inc.) with a laser source excitation wavelength of 532 nm under ambient conditions at room temperature. A 40× objective lens was used to focus the laser at a particular spot on the MoS_2 film (∼1 μm spot radius). XPS of the MoS_2 films was performed with a Thermo Fisher Scientific X-ray photoelectron spectrometer system utilizing a monochromatic Al K-alpha radiation source. A pass energy of 50 eV with a 0.1 eV scanning step was used for photoelectron detection. XPS spectra were obtained with a beam spot size of 50 × 50 μm^2. All XPS spectra were calibrated using the carbon (C) 1s peak at a binding energy of 284.4 eV as a reference.

ASSOCIATED CONTENT

Supporting Information

The Supporting Information is available free of charge at https://pubs.acs.org/doi/10.1021/acsnano.2c00021.

Details on surface charge transfer doping with the BV dopants, diagram of pulse waveform for reliable inkjet printing, BV film formation depending on the ink solvent, ink jettability depending on the volume ratio of toluene to cyclohexylbenzene, electrical characteristics of the pristine MoS_2 FETs and BV-doped MoS_2 FETs by solution immersion and inkjet printing, electrical characteristics of MoS_2 FETs after immersing into pure toluene and the CHB–toluene mixed solvent, and electrical characteristics of the MoS_2 FETs before and after spatially controllable BV doping by inkjet printing (PDF)

AUTHOR INFORMATION

Corresponding Authors

Gyu Tae Kim – *School of Electrical Engineering, Korea University, Seoul 02841, Korea;* orcid.org/0000-0003-1966-8572; Email: gtkim@korea.ac.kr

Takhee Lee – *Department of Physics and Astronomy and Institute of Applied Physics, Seoul National University, Seoul 08826, Korea;* orcid.org/0000-0001-5988-5219; Email: tlee@snu.ac.kr

Seungjun Chung – *Soft Hybrid Materials Research Center, Korea Institute of Science and Technology, Seoul 02792, Korea; KHU-KIST Department of Converging Science and Technology, Kyung Hee University, Seoul 02447, Korea;* orcid.org/0000-0002-4867-4149; Email: seungjun@kist.re.kr

Authors

Inho Jeong – *Soft Hybrid Materials Research Center, Korea Institute of Science and Technology, Seoul 02792, Korea;*

https://doi.org/10.1021/acsnano.2c00021
ACS Nano 2022, 16, 6215–6223

School of Electrical Engineering, Korea University, Seoul 02841, Korea

Kyungjune Cho − *Soft Hybrid Materials Research Center, Korea Institute of Science and Technology, Seoul 02792, Korea*

Seobin Yun − *Soft Hybrid Materials Research Center, Korea Institute of Science and Technology, Seoul 02792, Korea*

Jiwon Shin − *Department of Physics and Astronomy and Institute of Applied Physics, Seoul National University, Seoul 08826, Korea*

Jaeyoung Kim − *Department of Physics and Astronomy and Institute of Applied Physics, Seoul National University, Seoul 08826, Korea*

Complete contact information is available at: https://pubs.acs.org/10.1021/acsnano.2c00021

Notes

The authors declare no competing financial interest.

ACKNOWLEDGMENTS

The authors appreciate the financial support from the National Research Foundation of Korea (NRF) grant funded by the Korean government (the Ministry of Science and ICT) (No. NRF-2020R1A2C4001948) and the Korea Institute of Science and Technology (KIST) Future Resource Research Program (2E31811). J.S., J.K., and T.L. appreciate the financial support of the National Research Foundation of Korea (NRF) grant (No. 2021R1A2C3004783) funded by the Ministry of Science and ICT of Korea.

REFERENCES

(1) Ganatra, R.; Zhang, Q. Few-Layer MoS_2: A Promising Layered Semiconductor. *ACS Nano* **2014**, *8*, 4074−4099.

(2) Chaves, A.; Azadani, J. G.; Alsalman, H.; da Costa, D. R.; Frisenda, R.; Chaves, A. J.; Song, S. H.; Kim, Y. D.; He, D.; Zhou, J.; Castellanos-Gomez, A.; Peeters, F. M.; Liu, Z.; Hinkle, C. L.; Oh, S. H.; Ye, P. D.; Koester, S. J.; Lee, Y. H.; Avouris, P.; Wang, X.; Low, T. Bandgap Engineering of Two-Dimensional Semiconductor Materials. *npj 2D Mater. Appl.* **2020**, *4*, 29.

(3) Hui, Y. Y.; Liu, X.; Jie, W.; Chan, N. Y.; Hao, J.; Hsu, Y. Te; Li, L. J.; Guo, W.; Lau, S. P. Exceptional Tunability of Band Energy in a Compressively Strained Trilayer MoS_2 Sheet. *ACS Nano* **2013**, *7*, 7126−7131.

(4) Ferrari, A. C.; Bonaccorso, F.; Fal'ko, V.; Novoselov, K. S.; Roche, S.; Bøggild, P.; Borini, S.; Koppens, F. H. L.; Palermo, V.; Pugno, N.; et al. Science and Technology Roadmap for Graphene, Related Two-Dimensional Crystals, and Hybrid Systems. *Nanoscale* **2015**, *7*, 4598−4810.

(5) Wang, Q. H.; Kalantar-Zadeh, K.; Kis, A.; Coleman, J. N.; Strano, M. S. Electronics and Optoelectronics of Two-Dimensional Transition Metal Dichalcogenides. *Nat. Nanotechnol.* **2012**, *7*, 699−712.

(6) Yu, Z.; Ong, Z. Y.; Li, S.; Xu, J.-B.; Zhang, G.; Zhang, Y. W.; Shi, Y.; Wang, X. Analyzing the Carrier Mobility in Transition-Metal Dichalcogenide MoS_2 Field-Effect Transistors. *Adv. Funct. Mater.* **2017**, *27*, 1604093.

(7) Chen, X.; Park, Y. J.; Kang, M.; Kang, S. K.; Koo, J.; Shinde, S. M.; Shin, J.; Jeon, S.; Park, G.; Yan, Y.; MacEwan, M. R.; Ray, W. Z.; Lee, K. M.; Rogers, J. A.; Ahn, J. H. CVD-Grown Monolayer MoS_2 in Bioabsorbable Electronics and Biosensors. *Nat. Commun.* **2018**, *9*, 1690.

(8) Amani, M.; Chin, M. L.; Birdwell, A. G.; O'Regan, T. P.; Najmaei, S.; Liu, Z.; Ajayan, P. M.; Lou, J.; Dubey, M. Electrical Performance of Monolayer MoS_2 Field-Effect Transistors Prepared by Chemical Vapor Deposition. *Appl. Phys. Lett.* **2013**, *102*, 193107.

(9) Zhai, X.; Zhai, X.; Xu, X.; Peng, J.; Peng, J.; Jing, F.; Jing, F.; Zhang, Q.; Liu, H.; Liu, H.; Liu, H.; Hu, Z.; Hu, Z. Enhanced Optoelectronic Performance of CVD-Grown Metal-Semiconductor $NiTe_2/MoS_2$ Heterostructures. *ACS Appl. Mater. Interfaces* **2020**, *12*, 24093−24101.

(10) Choi, W.; Choudhary, N.; Han, G. H.; Park, J.; Akinwande, D.; Lee, Y. H. Recent Development of Two-Dimensional Transition Metal Dichalcogenides and Their Applications. *Mater. Today* **2017**, *20*, 116−130.

(11) Conti, S.; Pimpolari, L.; Calabrese, G.; Worsley, R.; Majee, S.; Polyushkin, D. K.; Paur, M.; Pace, S.; Keum, D. H.; Fabbri, F.; Iannaccone, G.; Macucci, M.; Coletti, C.; Mueller, T.; Casiraghi, C.; Fiori, G. Low-Voltage 2D Materials-Based Printed Field-Effect Transistors for Integrated Digital and Analog Electronics on Paper. *Nat. Commun.* **2020**, *11*, 3566.

(12) Migliato Marega, G.; Zhao, Y.; Avsar, A.; Wang, Z.; Tripathi, M.; Radenovic, A.; Kis, A. Logic-in-Memory Based on an Atomically Thin Semiconductor. *Nature* **2020**, *587*, 72−77.

(13) Gao, L.; Liao, Q.; Zhang, X.; Liu, X.; Gu, L.; Liu, B.; Du, J.; Ou, Y.; Xiao, J.; Kang, Z.; Zhang, Z.; Zhang, Y. Defect-Engineered Atomically Thin MoS_2 Homogeneous Electronics for Logic Inverters. *Adv. Mater.* **2020**, *32*, 1906646.

(14) Zhao, Y.; Xu, K.; Pan, F.; Zhou, C.; Zhou, F.; Chai, Y. Doping, Contact and Interface Engineering of Two-Dimensional Layered Transition Metal Dichalcogenides Transistors. *Adv. Funct. Mater.* **2017**, *27*, 1603484.

(15) Taghinejad, H.; Rehn, D. A.; Muccianti, C.; Eftekhar, A. A.; Tian, M.; Fan, T.; Zhang, X.; Meng, Y.; Chen, Y.; Nguyen, T. V.; Shi, S. F.; Ajayan, P. M.; Schaibley, J.; Reed, E. J.; Adibi, A. Defect-Mediated Alloying of Monolayer Transition-Metal Dichalcogenides. *ACS Nano* **2018**, *12*, 12795−12804.

(16) Mouri, S.; Miyauchi, Y.; Matsuda, K. Tunable Photoluminescence of Monolayer MoS_2 via Chemical Doping. *Nano Lett.* **2013**, *13*, 5944−5948.

(17) Kim, J. K.; Cho, K.; Jang, J.; Baek, K. Y.; Kim, J.; Seo, J.; Song, M.; Shin, J.; Kim, J.; Parkin, S. S. P.; Lee, J. H.; Kang, K.; Lee, T. Molecular Dopant-Dependent Charge Transport in Surface-Charge-Transfer-Doped Tungsten Diselenide Field Effect Transistors. *Adv. Mater.* **2021**, *33*, 2101598.

(18) Sim, D. M.; Kim, M.; Yim, S.; Choi, M. J.; Choi, J.; Yoo, S.; Jung, Y. S. Controlled Doping of Vacancy-Containing Few-Layer MoS_2 *via* Highly Stable Thiol-Based Molecular Chemisorption. *ACS Nano* **2015**, *9*, 12115−12123.

(19) Liu, X.; Qu, D.; Ryu, J.; Ahmed, F.; Yang, Z.; Lee, D.; Yoo, W. J. P-Type Polar Transition of Chemically Doped Multilayer MoS_2 Transistor. *Adv. Mater.* **2016**, *28*, 2345−2351.

(20) Kang, D. H.; Shim, J.; Jang, S. K.; Jeon, J.; Jeon, M. H.; Yeom, G. Y.; Jung, W. S.; Jang, Y. H.; Lee, S.; Park, J. H. Controllable Nondegenerate p-Type Doping of Tungsten Diselenide by Octadecyltrichlorosilane. *ACS Nano* **2015**, *9*, 1099−1107.

(21) Kang, D. H.; Kim, M. S.; Shim, J.; Jeon, J.; Park, H. Y.; Jung, W. S.; Yu, H. Y.; Pang, C. H.; Lee, S.; Park, J. H. High-Performance Transition Metal Dichalcogenide Photodetectors Enhanced by Self-Assembled Monolayer Doping. *Adv. Funct. Mater.* **2015**, *25*, 4219−4227.

(22) Luo, W.; Zhu, M.; Peng, G.; Zheng, X.; Miao, F.; Bai, S.; Zhang, X. A.; Qin, S. Carrier Modulation of Ambipolar Few-Layer $MoTe_2$ Transistors by MgO Surface Charge Transfer Doping. *Adv. Funct. Mater.* **2018**, *28*, 1704539.

(23) Khalil, H. M. W.; Khan, M. F.; Eom, J.; Noh, H. Highly Stable and Tunable Chemical Doping of Multilayer WS_2 Field Effect Transistor: Reduction in Contact Resistance. *ACS Appl. Mater. Interfaces* **2015**, *7*, 23589−23596.

(24) Chee, S. S.; Oh, C.; Son, M.; Son, G. C.; Jang, H.; Yoo, T. J.; Lee, S.; Lee, W.; Hwang, J. Y.; Choi, H.; Lee, B. H.; Ham, M. H. Sulfur Vacancy-Induced Reversible Doping of Transition Metal Disulfides *via* Hydrazine Treatment. *Nanoscale* **2017**, *9*, 9333−9339.

(25) Andleeb, S.; Kumar Singh, A.; Eom, J. Chemical Doping of MoS_2 Multilayer by p-Toluene Sulfonic Acid. *Sci. Technol. Adv. Mater.* **2015**, *16*, 035009.
(26) Yang, L.; Majumdar, K.; Liu, H.; Du, Y.; Wu, H.; Hatzistergos, M.; Hung, P. Y.; Tieckelmann, R.; Tsai, W.; Hobbs, C.; Ye, P. D. Chloride Molecular Doping Technique on 2D Materials: WS_2 and MoS_2. *Nano Lett.* **2014**, *14*, 6275−6280.
(27) Fang, H.; Tosun, M.; Seol, G.; Chang, T. C.; Takei, K.; Guo, J.; Javey, A. Degenerate n-Doping of Few-Layer Transition Metal Dichalcogenides by Potassium. *Nano Lett.* **2013**, *13*, 1991−1995.
(28) Kiriya, D.; Tosun, M.; Zhao, P.; Kang, J. S.; Javey, A. Air-Stable Surface Charge Transfer Doping of MoS_2 by Benzyl Viologen. *J. Am. Chem. Soc.* **2014**, *136*, 7853−7856.
(29) Chamlagain, B.; Withanage, S. S.; Johnston, A. C.; Khondaker, S. I. Scalable Lateral Heterojunction by Chemical Doping of 2D TMD Thin Films. *Sci. Rep.* **2020**, *10*, 12970.
(30) Chen, M.; Nam, H.; Wi, S.; Ji, L.; Ren, X.; Bian, L.; Lu, S.; Liang, X. Stable Few-Layer MoS_2 Rectifying Diodes Formed by Plasma-Assisted Doping. *Appl. Phys. Lett.* **2013**, *103*, 142110.
(31) Choi, M. S.; Qu, D.; Lee, D.; Liu, X.; Watanabe, K.; Taniguchi, T.; Yoo, W. J. Lateral MoS_2 p-n Junction Formed by Chemical Doping for Use in High-Performance Optoelectronics. *ACS Nano* **2014**, *8*, 9332−9340.
(32) Khim, D.; Baeg, K. J.; Caironi, M.; Liu, C.; Xu, Y.; Kim, D. Y.; Noh, Y. Y. Control of Ambipolar and Unipolar Transport in Organic Transistors by Selective Inkjet-Printed Chemical Doping for High Performance Complementary Circuits. *Adv. Funct. Mater.* **2014**, *24*, 6252−6261.
(33) Shimizu, R.; Matsuzaki, S.; Yanagi, K.; Takenobu, T. Optical Signature of Charge Transfer in n-Type Carbon Nanotube Transistors Doped with Printable Organic Molecules. *Appl. Phys. Express* **2012**, *5*, 125102.
(34) Kim, H.; Choi, W. S. Controlled Zr Doping for Inkjet-Printed ZTO TFTs. *Ceram. Int.* **2017**, *43*, 4775−4779.
(35) Kim, T. Y.; Ha, J.; Cho, K.; Pak, J.; Seo, J.; Park, J.; Kim, J. K.; Chung, S.; Hong, Y.; Lee, T. Transparent Large-Area MoS_2 Phototransistors with Inkjet-Printed Components on Flexible Platforms. *ACS Nano* **2017**, *11*, 10273−10280.
(36) Liu, J.; Sun, K.; Zheng, X.; Wang, S.; Lian, S.; Deng, C.; Xie, H.; Zhang, X.; Gao, Y.; Song, F.; Huang, H. Evolutions of Morphology and Electronic Properties of Few-Layered MoS_2 Exposed to UVO. *Results Phys.* **2020**, *19*, 103634.
(37) Shao, P. Z.; Zhao, H. M.; Cao, H. W.; Wang, X. F.; Pang, Y.; Li, Y. X.; Deng, N. Q.; Zhang, J.; Zhang, G. Y.; Yang, Y.; Zhang, S.; Ren, T. L. Enhancement of Carrier Mobility in MoS_2 Field Effect Transistors by a SiO_2 Protective Layer. *Appl. Phys. Lett.* **2016**, *108*, 203105.
(38) Yue, D.; Kim, C.; Lee, K. Y.; Yoo, W. J. Ohmic Contact in 2D Semiconductors via the Formation of a Benzyl Viologen Interlayer. *Adv. Funct. Mater.* **2019**, *29*, 1807338.
(39) Mercado, E.; Goodyear, A.; Moffat, J.; Cooke, M.; Sundaram, R. S. A Raman Metrology Approach to Quality Control of 2D MoS_2 Film Fabrication. *J. Phys. D. Appl. Phys.* **2017**, *50*, 184005.
(40) Kim, J. G.; Yun, W. S.; Jo, S.; Lee, J.; Cho, C. H. Effect of Interlayer Interactions on Exciton Luminescence in Atomic-Layered MoS_2 Crystals. *Sci. Rep.* **2016**, *6*, 29813.
(41) Sun, L.; Zhang, X.; Liu, F.; Shen, Y.; Fan, X.; Zheng, S.; Thong, J. T. L.; Liu, Z.; Yang, S. A.; Yang, H. Y. Vacuum Level Dependent Photoluminescence in Chemical Vapor Deposition-Grown Monolayer MoS_2. *Sci. Rep.* **2017**, *7*, 16714.
(42) Chakraborty, B.; Bera, A.; Muthu, D. V. S.; Bhowmick, S.; Waghmare, U. V.; Sood, A. K. Symmetry-Dependent Phonon Renormalization in Monolayer MoS_2 Transistor. *Phys. Rev. B* **2012**, *85*, 161403.
(43) Kukucska, G.; Koltai, J. Theoretical Investigation of Strain and Doping on the Raman Spectra of Monolayer MoS_2. *Phys. Status Solidi B* **2017**, *254*, 1700184.
(44) Hernández-Alonso, M. D.; Fresno, F.; Suárez, S.; Coronado, J. M. Development of Alternative Photocatalysts to TiO_2: Challenges and Opportunities. *Energy Environ. Sci.* **2009**, *2*, 1231−1257.
(45) López-Cabaña, Z.; Navas, D.; Benavente, E.; Ana, M. A. S.; Lavayen, V.; González, G. Hybrid Laminar Organic-Inorganic Semiconducting Nanocomposites. *Mol. Cryst. Liq. Cryst.* **2012**, *554*, 119−134.
(46) Kim, S. M.; Jang, J. H.; Kim, K. K.; Park, H. K.; Bae, J. J.; Yu, W. J.; Lee, I. H.; Kim, G.; Loc, D. D.; Kim, U. J.; Lee, E. H.; Shin, H. J.; Choi, J. Y.; Lee, Y. H. Reduction-Controlled Viologen in Bisolvent as an Environmentally Stable n-Type Dopant for Carbon Nanotubes. *J. Am. Chem. Soc.* **2009**, *131*, 327−331.
(47) Nallan, H. C.; Sadie, J. A.; Kitsomboonloha, R.; Volkman, S. K.; Subramanian, V. Systematic Design of Jettable Nanoparticle-Based Inkjet Inks: Rheology, Acoustics, and Jettability. *Langmuir* **2014**, *30*, 13470−13477.
(48) McKinley, G. H.; Renardy, M. Wolfgang von Ohnesorge. *Phys. Fluids* **2011**, *23*, 127101.
(49) Derby, B. Inkjet Printing of Functional and Structural Materials: Fluid Property Requirements, Feature Stability, and Resolution. *Annu. Rev. Mater. Res.* **2010**, *40*, 395−414.
(50) Liu, Y.; Li, F.; Xu, Z.; Zheng, C.; Guo, T.; Xie, X.; Qian, L.; Fu, D.; Yan, X. Efficient All-Solution Processed Quantum Dot Light Emitting Diodes Based on Inkjet Printing Technique. *ACS Appl. Mater. Interfaces* **2017**, *9*, 25506−25512.
(51) Hahm, D.; Park, J.; Jeong, I.; Rhee, S.; Lee, T.; Lee, C.; Chung, S.; Bae, W. K.; Lee, S. Surface Engineered Colloidal Quantum Dots for Complete Green Process. *ACS Appl. Mater. Interfaces* **2020**, *12*, 10563−10570.
(52) Lee, D.; Lee, J. J.; Kim, Y. S.; Kim, Y. H.; Kim, J. C.; Huh, W.; Lee, J.; Park, S.; Jeong, H. Y.; Kim, Y. D.; Lee, C. H. Remote Modulation Doping in van Der Waals Heterostructure Transistors. *Nat. Electron.* **2021**, *4*, 664−670.
(53) Mawlong, L. P. L.; Bora, A.; Giri, P. K. Coupled Charge Transfer Dynamics and Photoluminescence Quenching in Monolayer MoS_2 Decorated with WS_2 Quantum Dots. *Sci. Rep.* **2019**, *9*, 19414.
(54) Mak, K. F.; He, K.; Lee, C.; Lee, G. H.; Hone, J.; Heinz, T. F.; Shan, J. Tightly Bound Trions in Monolayer MoS_2. *Nat. Mater.* **2013**, *12*, 207−211.
(55) Cao, L.; Fang, G.; Wang, Y. Electroreduction of Viologen Phenyl Diazonium Salts as a Strategy to Control Viologen Coverage on Electrodes. *Langmuir* **2017**, *33*, 980−987.
(56) Zhang, S.; Hill, H. M.; Moudgil, K.; Richter, C. A.; Hight Walker, A. R.; Barlow, S.; Marder, S. R.; Hacker, C. A.; Pookpanratana, S. J. Controllable, Wide-Ranging n-Doping and p-Doping of Monolayer Group 6 Transition-Metal Disulfides and Diselenides. *Adv. Mater.* **2018**, *30*, 1802991.

https://doi.org/10.1021/acsnano.2c00021
ACS Nano 2022, 16, 6215−6223